Heliyon 10 (2024) e39063

Contents lists available at ScienceDirect

Heliyon

journal homepage: www.cell.com/heliyon

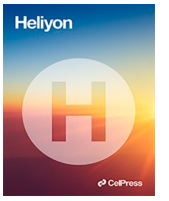

Research article

Fabrication and characterization of reinforced glass ionomer cement by zinc oxide and hydroxyapatite nanoparticles

Reyhaneh Azimi [a], Mohamad Shahgholi [a,*], Amirsalar Khandan [b,**]

[a] Department of Mechanical Engineering, Najafabad Branch, Islamic Azad University, Najafabad, Iran
[b] Dental Research Center, Department of Endodontics, Dental Research Institute, School of Dentistry, Isfahan University of Medical Sciences, Isfahan, Iran

ARTICLE INFO

Keywords:
Reinforced bone cement
Glass ionomer
ZnO nanoparticles
Biomaterial characterization

ABSTRACT

This study shows the enhancement of glass ionomer cement (GIC) by incorporating hydroxyapatite (HA) and zinc oxide (ZnO) nanoparticles to improve its mechanical strength, biological activity, and antibacterial properties. GC is widely used in dental and orthopedic applications due to its bioactivity and biocompatibility, but it suffers from weak antibacterial properties and limited load-bearing capacity. HA, a calcium phosphate compound similar to natural bone, and ZnO, known for its antibacterial and bone-regenerative properties, were integrated into GIC to address these limitations. The modified GC exhibited improved compressive strength and bioactivity, particularly with the addition of 4 wt% ZnO nanoparticles, which showed the highest increase in mechanical performance while maintaining cytocompatibility. However, the fluoride release was reduced, indicating an exchange between enhanced mechanical properties and fluoride ion release. Antibacterial efficacy was assessed using well diffusion, MIC, and MBC tests, confirming that the modified GC has significant potential in dental and orthopedic applications. Future research should focus on the long-term effects of Zn^{2+} ion release to fully understand its impact on the antibacterial performance of the cement.

1. Introduction

Reinforced bone cement, incorporating Glass Ionomer and ZnO nanoparticles, enhances the mechanical properties and bioactivity of orthopedic materials, offering improved strength, durability, and compatibility for effective bone repair and regeneration in medical applications.

One treatment method for bone tissue diseases involves the use of biomaterials. The effectiveness of biomaterials depends on several key factors, including the biocompatibility of the implant, the patient's health status, and the surgical method used for implantation, which governs the process [1]. Hydroxyapatite (HA), a biocompatible biomaterial, is the primary mineral component of both tooth enamel and bone tissue. HA is a biocompatible material and a primary inorganic component of tooth enamel and bone tissue. HA constitutes the main mineral phase in bone and tooth cells, making it a well-known bone substitute or repair material for bone and teeth. This is due to its various desirable properties, including anti-carcinogenicity, biocompatibility, low thermal expansion coefficient, low thermal conductivity, antimicrobial properties, and structural similarity to human teeth and the skeletal system [2,3].

* Corresponding author.
** Corresponding author.
E-mail address: mohamad.shahgholi@gmail.com (M. Shahgholi).

https://doi.org/10.1016/j.heliyon.2024.e39063
Received 30 April 2024; Received in revised form 23 September 2024; Accepted 7 October 2024
Available online 9 October 2024

HA is the most widely used calcium phosphate in dental and bone implant materials due to its antibacterial properties, which help prevent infections post-implantation [4]. However, HA lacks sufficient mechanical strength because of its crystalline structure [5]. Among single-phase calcium phosphates, HA is the most stable and least soluble, with a solubility value of about 2.9×10^{-58} in the pH range of 3.5–9.7. Despite its low solubility, HA particles can serve as nucleation sites for apatite crystal precipitation in calcium and phosphate ion-saturated culture mediums.

HA is known for being osteoconductive but not osteoinductive. Enhancements in the physical, chemical, solubility, and bioactivity properties of HA can be achieved through ion substitution [6]. Nano-HA, a relatively new material, exhibits superior physical, chemical, mechanical, and biological properties compared to traditional HA, making it suitable for various interventions. As a tissue engineering material, Nano-HA enhances bone regeneration better than autologous bone grafts and is used in fields such as immunology, surgery, periodontology, and aesthetics [7]. HA inherently lacks significant antibacterial properties. However, these properties can be enhanced by incorporating mineral ions with known antibacterial effects. Studies have demonstrated that integrating metal ions such as silver nanoparticles, CuO nanoparticles, and ZnO nanoparticles into the HA structure markedly improves antibacterial efficacy [8]. Furthermore, the mechanical properties and biological performance of HA can be enhanced by the addition of bioactive ions like magnesium, or other elements such as Zinc and Strontium [9].

It shows that zinc is one of the important components in bones.

Zinc ion (Zn^{2+}) is one of the important components in bones stimulating effect on the bone mineral deposition process, in vitro and in vivo [10]. Zn^{2+} is effective in improving the mechanical and biological properties of HA. As an essential element in the human body, Zn^{2+} supports the immune system, cell division, fertility, growth, and maintenance of healthy bones [11]. Zn^{2+} is one of the best semiconductor materials due to its biocompatibility, superior physicochemical properties [12]. Zn^{2+} is particularly noted for its anti-osteoporosis properties, making it valuable in treating osteoporosis, orthopedic conditions, bone defects, and spinal fusion cases [13]. Zn^{2+} also promotes bone formation and inhibits osteoclast activity in vitro [14]. Zn^{2+} has anti-inflammatory and antibacterial properties, thus facilitating bone healing. In addition, it also increases bone density. The presence of Zn^{2+} in glass increases its mechanical and chemical strength and reduces its durability and degradability in aqueous environments such as simulated body fluid (SBF) [10]. Incorporating zinc oxide (ZnO) with HA decreases crystallinity and enhances bacterial inhibition [15]. Additionally, ZnO added to HA can inhibit biofilm formation and promote osteoblast proliferation [16,17]. Glass-ionomer cements (GICs), introduced in the mid-1970s, have been extensively improved to enhance their strength and are widely used in clinical applications. However, their use is limited to low-load areas. Conventional GICs have been the focus of much research [17]. GICs are semi-transparent like dental porcelain and adhere well to teeth, offering beneficial vital activities [18]. They are used for fillings, cappings, and bonding restorations [19], and their unique properties such as high dielectric constant, non-toxicity, high biocompatibility, mechanical strength, and fluoride release—make them suitable for tooth and bone restoration [13]. The fluoride ion release from GICs helps prevent the decay of surrounding tissues and enhances their antimicrobial properties by reducing demineralization [20–22].

Despite their benefits, GICs have limitations, including insufficient mechanical resistance, long hardening times, sensitivity to moisture, surface roughness, inadequate strength, high wear, dullness, and short working times, secondary decay, and low bioactivity. Many of these issues have been addressed in newer formulations of GICs, which now rely on an acid-base reaction for hardening and cement formation. These improved GICs are widely used in tooth and bone restorative applications. Researchers continually work to optimize their properties, incorporating HA into GICs to increase compressive and shear strength [12,23–29]. Studies have shown that GICs with nano-HA exhibit greater resistance to demineralization compared to those with micro-HA [29,30]. Adding HA nanoparticles to GICs enhances fluoride ion release, mechanical properties, and antibacterial activity, making them suitable for clinical use [19–24].

Research has demonstrated that ZnO-HA NPs embedded in GIC, fabricated using ultrasonication, significantly delay microbial activity [3]. Based on these results, a biocompatible cement with suitable mechanical strength, impact durability, bioactivity, and bacterial inhibition is highly desirable for bone and tooth tissue replacements. This study aims to introduce such a cement with favorable mechanical and biological properties for these applications. The primary aim of this study is to enhance the mechanical strength and biological activity of glass ionomer cement (GIC) by reinforcing it with HA nanoparticles and ZnO ions. This research focuses on evaluating the synergistic effects of these reinforcements at various concentrations, which has not been extensively explored in existing literature. The novelty lies in the comprehensive analysis of how these additions influence the porosity, holding time, bioactivity, and antibacterial properties of GC, while also examining their impact on fluoride release and cytotoxicity. The results contribute significantly by demonstrating that the incorporation of ZnO nanoparticles not only boosts the strength and biological viability of the cement but also provides a new perspective on optimizing glass ionomer formulations for enhanced clinical performance. This research shows how the incorporation of HA and ZnO can improve the physical properties of GIC while maintaining its biocompatibility and introducing antibacterial properties.

2. Materials and methods

2.1. Preparation of cement powder

Reinforcement of glass ionomer cement (GIC) may expand its applications, especially for posterior teeth [17]. HA and ZnO powder were obtained from Merck, Germany, 98 % purity. GC powder was sourced from GC Corporation, Japan. The first step is the preparation of the cement powder, composed of GC (90 wt%) and nano HA (10 wt%) using a planetary ball mill (model Fp4). The conditions in ball milling that influence the mechanical process include the type of balls, the filling ratio, and the rotation speed [28]. Initially, 26.1 g of GC and 2.9 g of HA were placed in a ball mill containing alumina pellets at a ratio of 1:10, milled for 30 min at a speed of 450 rpm. The resultant powder, named Hydroxyapatite Glass Ionomer Cement (HGIC), was extracted from the mill. A

Sartorius digital scale with an accuracy of 0.0001 g was used for precise measurement of materials. At this stage, a planetary ball mill was used to ensure a uniform particle size distribution of GC, HA, and ZnO powder. The second step involved preparing HA powder with varying percentages of ZnO along with GC powder. Three different experimental specimens were created by varying the percentage of HA nanoparticles while maintaining constant ZnO percentages (2 wt%, 4 wt%, and 6 wt%). These specimens were prepared using a high-energy ball milling method for 15 min. The ZnO/HA combination demonstrates antibacterial efficacy, although no correlation between efficiency and Zn content was observed [21]. Subsequently, maintaining the GC at 90 wt%, the HA and ZnO compounds were combined using the ball mill for 30 min at a speed of 450 rpm. After 30 min, the powder was removed from the mill. To clarify the cement production procedure, all the steps are illustrated in Fig. 1(a–f).

2.2. XRD analysis

The properties of materials depend on whether they are crystalline or amorphous. To determine the phase, identify the type of material, and confirm its structure, X-ray diffraction (XRD) analysis was performed on the powder of the GC control sample as well as on samples combined with HA and ZnO-NPs. The results were analyzed using Expert High Score software version 3.0.5.

2.3. XRF analysis

X-ray Fluorescence (XRF) elemental analysis was used to identify the elements in cement powder and also to determine the quantitative and qualitative number of elements in GC cement powder and produced cement powder. This analysis was performed

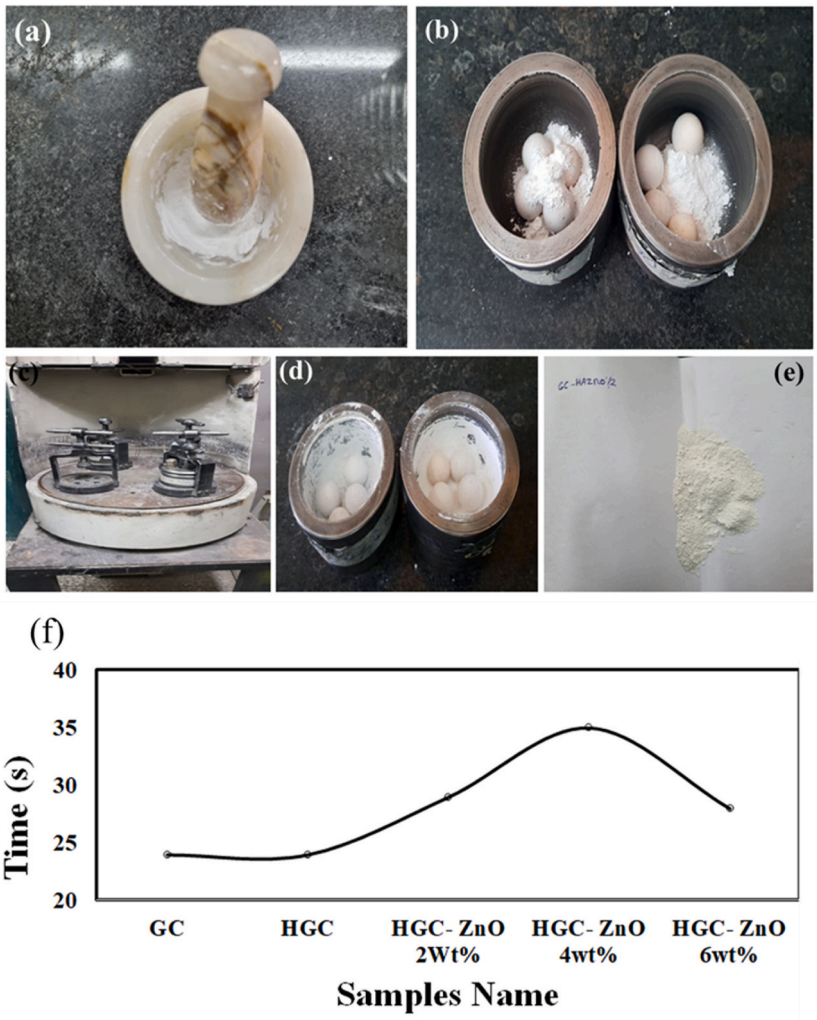

Fig. 1. a) Ball milling of ZnO and HA with a high energy ball mill; b) placing GC, HA, ZnO powder in a steel cup; c) placing the chambers containing cement in the ball mill machine, d) cement powder obtained after 30 min being placed in a ball mill machine with a speed of 450 rpm, and e) the final powder removed from the chambers (HGC-ZnO 2 wt%), f) Setting time for each sample.

using a Philips PW1480 XRF.

2.4. FESEM analysis

FESEM analysis was used to determine the size of cement powder particles and to prepare images of powder particles at high magnification and resolution. This analysis was performed using a Field Emission Scanning Electron Microscope (FESEM) model QUANTA FEG-450 made by FEI Company, USA. The characteristics of the fracture surface, microstructures, and morphology of the materials were investigated using a LEO 435VP SEM made in the Netherlands. FESEM and SEM images were analyzed using Image-J software in terms of particle size, microstructure, and porosity.

2.5. Sample preparation

In the stage of making bone cement samples, first, the GC powder phase was mixed with its liquid phase in a ratio of 2:1 to make bone cement samples. Then, the paste material obtained by mixing the powder phase and liquid cement was poured into the mold. Cement setting time was measured using a Vicat needle. The mold was placed in a hydraulic pressure machine (SANTAM-STM20) with a pressure of 50 MPa. The steps of making the sample can be seen in Fig. 2(a and b) and Fig. 3. In addition, the naming of the samples based on their ingredients is stated in Table 1

This type of destructive testing is commonly used to evaluate the mechanical properties and load-bearing capacity of materials, components, or structures. The broken and distorted appearance of the specimen in the image illustrates the extent of deformation and failure that occurred under the compressive stresses.

2.6. Mechanical strength experiment

The used repair materials often replace the tissue and are subject to tension and bending [29]. Bone cements are weak in terms of tensile strength, but usually much stronger in terms of compressive strength and must have adequate mechanical strength against pressure and impact. can be used in the treatment of bone and dental diseases [30,31]. The factors that affect the mechanical properties are the ratio of the sample dimensions, the percentage of porosity, the scaffold construction method, and its ingredients [32]. The experiments have done based on the movement control method on standard dimensions' samples. The ratio of height to diameter and grip speed are relatively 2:1 and 5 mm/s. The fracture surface of the samples was examined to the degree of porosity and the type of fracture.

2.7. Bioactivity evaluation

Examining the bioactivity of bone cement is very important. To investigate the bioactivity of cement and the effect of adding HA and ZnO to GC, the samples were placed in an incubator at 37 °C for 28 days in SBF solution. The pH of the solution of each sample was measured using a pH meter and pH paper in 1, 4, 7, 14, 21 and 28 days. After the bioactivity assessment of the samples, they were again analyzed by SEM to observe the formation and growth of calcium.

2.8. FTIR analysis

The samples were analyzed by Fourier transform infrared spectrometer (FTIR) analysis to detect functional groups, determine the structure of organic compounds, identify chemical bonds, determine the correctness of a chemical reaction, and determine the progress

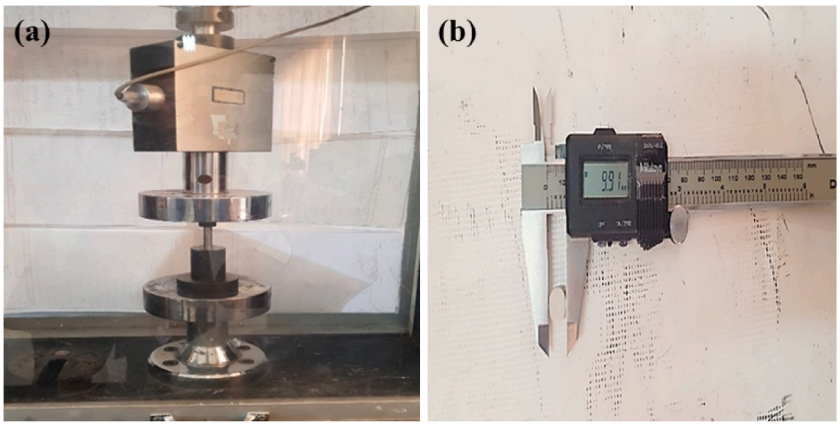

Fig. 2. Bone cement specimens a) the mold placed in the pressure device and b) cement specimen after removing from the mold.

Fig. 3. The broken specimens after performing the compressive strength examination.

Table 1
Materials used in the specimens formation.

Specimen name	Variable structure of specimens
GC	Glass ionomer
HGC	Glass ionomer + HA
HGC-ZnO 2 wt%	Glass ionomer + HA + ZnO 2 wt%
HGC-ZnO 4 wt%	Glass ionomer + HA + ZnO 2 wt%
HGC-ZnO 6 wt%	Glass ionomer + HA + ZnO 6 wt%

of various reactions after bioactivity. This analysis was performed using a FTIR model Tensor 27 made by Bruker.

2.9. Fluoride release evaluation

Examining the release of fluoride is very important because the fluoride ion has antibacterial properties that prevent caries. The amount of fluoride released protects the tissue around the cement against decay. To measure the amount of fluoride released, a period of 28 days was considered based on the standard method of 4500 F-D. The amount of fluoride released from the samples was measured on the 1st and 28th days.

2.10. Biodegradability assessment

When bone cements are used in bone reconstruction, the cement is destroyed and replaced with living tissue. The rate of degradation of cement is similar to the rate of new bone formation. To evaluate the degradability of the samples, they were placed in an incubator at 37 °C for 28 days in phosphate buffer saline (PBS) solution. The weight of the samples was measured on days 1, 4, 7, 14, 21, and 28 with a scale with 2 decimal places.

2.11. Antibacterial examination

2.11.1. Antibiogram test to Rochelle diffusion-test on sample

The growth of bacteria was assessed for each sample using the antibiogram examination with the well diffusion method - test on the sample (ISIRI 13560). *Staphylococcus aureus* 6538 ATCC as gram-positive bacteria and *Escherichia coli* 10536 ATCC as gram-negative bacteria were cultured under suitable conditions in liquid medium at a temperature of 35 ± 2 °C for one day. A certain amount was removed from each bacteria cultured in liquid culture medium and cultured on solid culture medium to obtain isolated colonies. A part of the bacterial colony was removed after bacterial isolation in the microbial solid culture medium and dissolved in sterile serum. Also, the final concentration of bacteria in each test tube was prepared after preparing a homogeneous solution equivalent to half of McFarland. Then, the solution was mixed with a sterilized swab and the grass was cultured with the swab on the microbial solid culture medium. After culture, the samples tested for antibiogram were transferred to the culture medium and incubated for 24 h at 37 °C. After 24 h, the plate was examined and the area of growth inhibition zone was measured.

2.11.2. Antibacterial test by MIC/MBC method

Staphylococcus aureus ATCC6538 as Gram-positive bacteria and *Escherichia coli* ATCC10536 as Gram-negative bacteria were cultured in liquid medium at a temperature of 37 ± 2 °C for one day and night under suitable conditions. A specified amount of inoculum was removed from each bacterium in the culture medium. A specified amount of sample and culture medium was poured into each test tube and a serial dilution of the sample was prepared. The final concentration of bacteria in each test tube is equal to half of McFarland. The culture medium was considered as a negative quality control and the culture medium with bacterial suspension was considered as a positive control. All the tubes were placed in a greenhouse at a temperature of 37 ± 2 °C and after 24 h they were assessed for the presence or absence of turbidity (MIC test). After this period, the samples in the tubes were cultured in the culture

medium containing agar and any growth was reported (MBC test). All samples underwent a 24-h incubation for assessment in both the MIC and MBC tests.

2.12. MTT analysis

Some biomaterials in the body may cause immune reactions. For this reason, before transferring these substances to the body, their various properties, especially biocompatibility, should be assessed. Cytotoxicity of the samples HGC, HGC-ZnO 2 wt%, HGC-ZnO 4 wt %, HGC-ZnO 6 wt% in the suitable environment according to ISO 10993-5:2009 standard after 24 ± 2, 48 ± 2, 72 ± 2 h was performed on MG63 cells.

2.13. Setting time investigation

Several factors influence the setting time of cement, including the powder-to-liquid ratio and particle size in the cement powder phase. The Vicat needle was used to measure the setting time. The setting time was consistent for GC and HGC specimens, but increased with the addition of ZnO. Given the short setting time of GC, extending the setting time remains a crucial consideration in specimen preparation (Fig. 1(f)).

3. Results and discussion

The incorporation of antimicrobial agents into GCs significantly impacts the physical and mechanical properties of the cement. Experimental findings confirm a decrease in compressive strength, surface hardness, and bond strength with increasing concentrations of antimicrobial agents. Moreover, higher concentrations lead to reduced setting times [15]. The enhanced antibacterial properties of the GIC reinforced with HA and ZnO nanoparticles can be attributed to several mechanisms. The release of Zn^{2+} from the ZnO nanoparticles can disrupt bacterial cell membranes, interfere with enzymatic activities, and inhibit bacterial proliferation, creating an unfavorable environment for both Gram-positive and Gram-negative bacteria. Additionally, the ZnO nanoparticles can generate reactive oxygen species that cause oxidative stress and damage bacterial cells, while the sharp edges and high surface area of the ZnO can physically disrupt the bacterial cell membranes. The HA itself also possesses some antibacterial activity, particularly against Gram-positive bacteria, due to its ability to adsorb and concentrate bacterial components on its surface.

3.1. XRD results

Fig. 4(a–g) shows the XRD results of HA, ZnO, GC powder, and the manufactured cement powders (HGC, HGC-ZnO 2 wt%, HGC-ZnO 4 wt%, HGC-ZnO 6 wt%). XRD analysis done using X pert high-score software. HA and ZnO show nanocrystalline structures, while GC is amorphous, characterized by an irregular structure. The patterns of HGC, HGC-ZnO 2 wt%, HGC-ZnO 4 wt%, and HGC-ZnO 6 wt

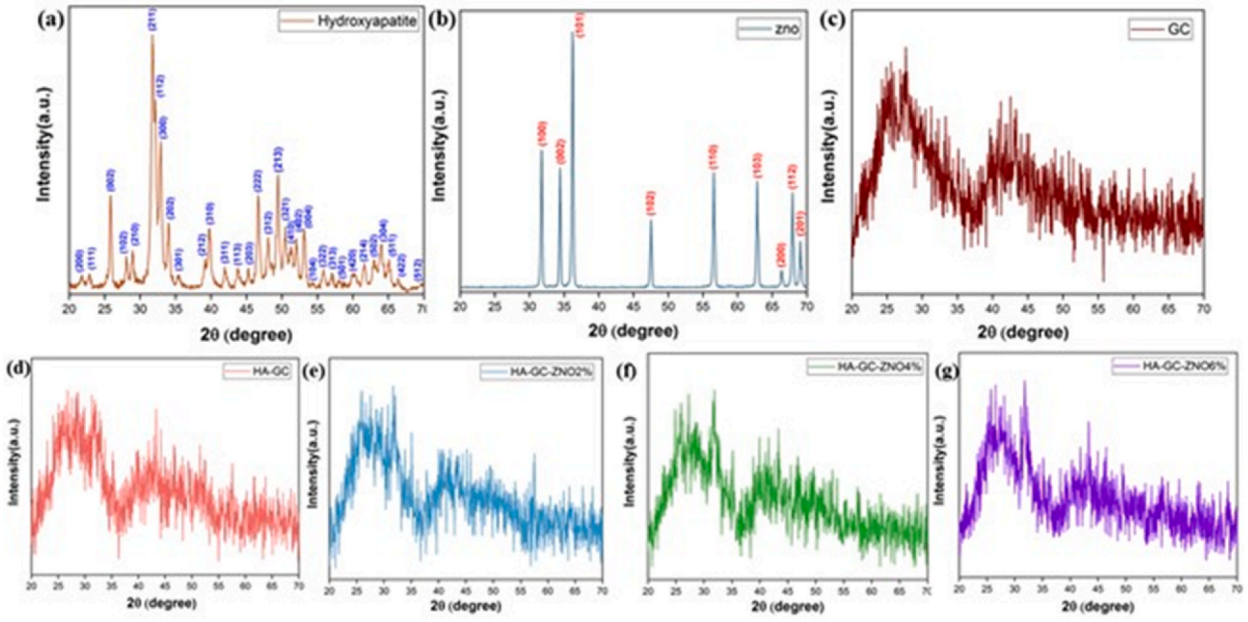

Fig. 4. The results of XRD pattern of the powder phase of specimens a) HA, b) ZnO, c) GC, d) HGC, e) HGC-ZnO 2 wt%, f) HGC-ZnO 4 wt%, and g) HGC-ZnO 6 wt%.

% lack specific order compared to HA and ZnO, due to GC constituting 90 % of these cements, imparting greater amorphous properties. Weak peaks in the patterns of these specimens confirm the presence of HA and ZnO nanoparticles. The presence of hydroxyapatite (HA) on the HGC specimen is indeed confirmed through XRD analysis, as depicted in Fig. 5. However, due to the relatively low concentration of HA (10 wt%) compared to the dominant glass ionomer matrix (90 wt%), the corresponding HA diffraction peaks are relatively weak and may appear less prominent in the diffraction pattern. Despite this, careful examination of the XRD pattern reveals the characteristic peaks of HA, indicating its formation. We acknowledge that a more detailed analysis or higher magnification could further enhance the visibility of these peaks.

3.2. XRF results

Fig. 6 shows the XRF analysis of SiO_2, Al_2O_3, Sr, F, P_2O_5, Na_2O, TiO_2, and Cu are the predominant elements in GC, with Cu present in trace amounts. Introducing HA ($Ca_{10}(PO_4)_6(OH)_2$) to GC through ball milling induces ion replacement and chemical reactions, altering ion concentrations. Sr and TiO_2 decrease upon HA addition, with further reductions seen in HA-ZnO 2 wt% and HA-ZnO 4 wt %, and an increase observed with HA-ZnO 6 wt%. SiO_2, Al_2O_3, and Na_2O levels remain relatively constant across all cements. F ion concentrations decrease progressively with HA and HA-ZnO additions, reaching zero in 6 wt% HGC-ZnO powder. P_2O_5 levels rise due to ion substitutions facilitated by HA. XRF limitations prevent the detection of elements lighter than sodium, such as hydrogen. Additionally, HGC-ZnO cement powder contains approximately 2 wt% Fe_2O_3 impurities, originating from pot abrasion during cement production.

3.3. FESEM results

The images acquired from FESEM are showed in Fig. 7(a–e). Image analysis was conducted using Image-J software, which calculated the average particle diameter. For the control specimen of GC without ball milling, the particle diameter measured 0.32 μm. The specimens where GC, HA, and ZnO powders were milled and combined showed a different particle size distribution. Table 2 shows the average particle diameters of each specimen.

3.4. SEM results

The specimens' substructure and morphology were examined using a scanning electron microscope before and after 28 days of immersion in simulated body fluid (SBF). Fig. 8(a–d) shows the porosity analysis conducted using Image-J software, with results detailed in Table 3.

Porosity influences biodegradation and osteogenesis [13], with increased porosity decreasing material strength under stress. The sample containing HA exhibited the highest porosity at 40 %, resulting in the lowest resistance to stress and crushing. Conversely, the addition of ZnO reduced porosity, increased compressive strength, and promoted calcium growth due to ZnO's bone growth properties. Fracture surface morphologies are depicted in Fig. 8(a–d) as GC shows cracks, HGC displays flaking, and HGC-ZnO 2 wt% exhibits holes and cracks, while HGC-ZnO 4 wt% and HGC-ZnO 6 wt% show cracks and flaking. Addition of HA to GC reduced crack size on the fracture surface (Fig. 8(a and b)), likely due to HGC's higher porosity. Fracture surfaces did not significantly differ with varying HA-ZnO percentages compared to HGC, although HA-ZnO specimens exhibited lower porosity. Thus, ZnO NPs effectively reduce porosity. Comparison of pre- and post-SBF immersion images in Fig. 8(a–d) indicates white sedimentation nanostructure reflecting apatite formation extent.

In GC specimens, HA growth appears as tiny buds, facilitating HA formation and growth. In ZnO-containing cements, HA growth changes from point to cauliflower shape with increasing ZnO percentage, enhancing HA growth in cauliflower morphology.

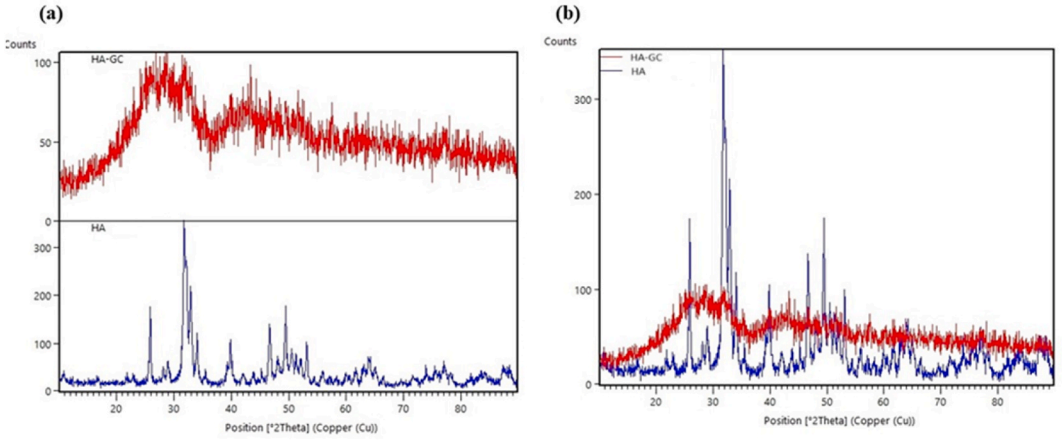

Fig. 5. The results of the XRD pattern of the powder phase of specimens a) HA and HGC Separately, b) Superposition of HA and HGC patterns.

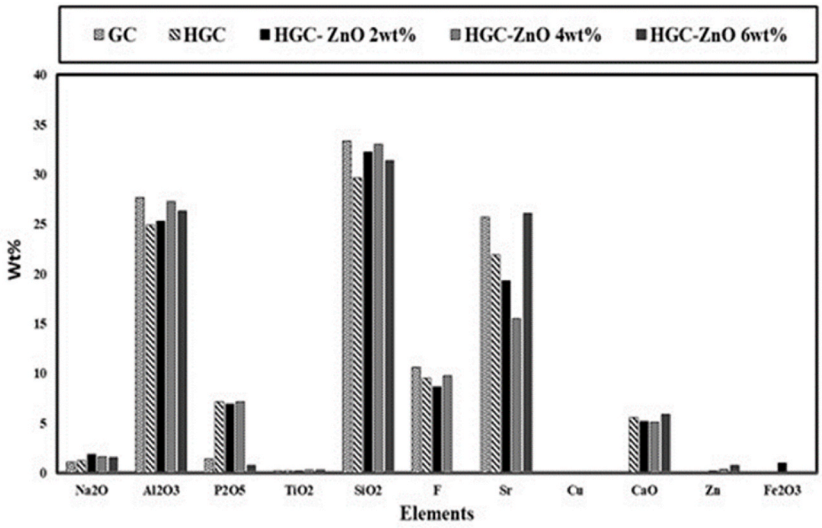

Fig. 6. Elemental analysis chart of GC, HGC, HGC-ZnO 2 wt%, HGC-ZnO 4 wt% and HGC-ZnO 6 wt% cements.

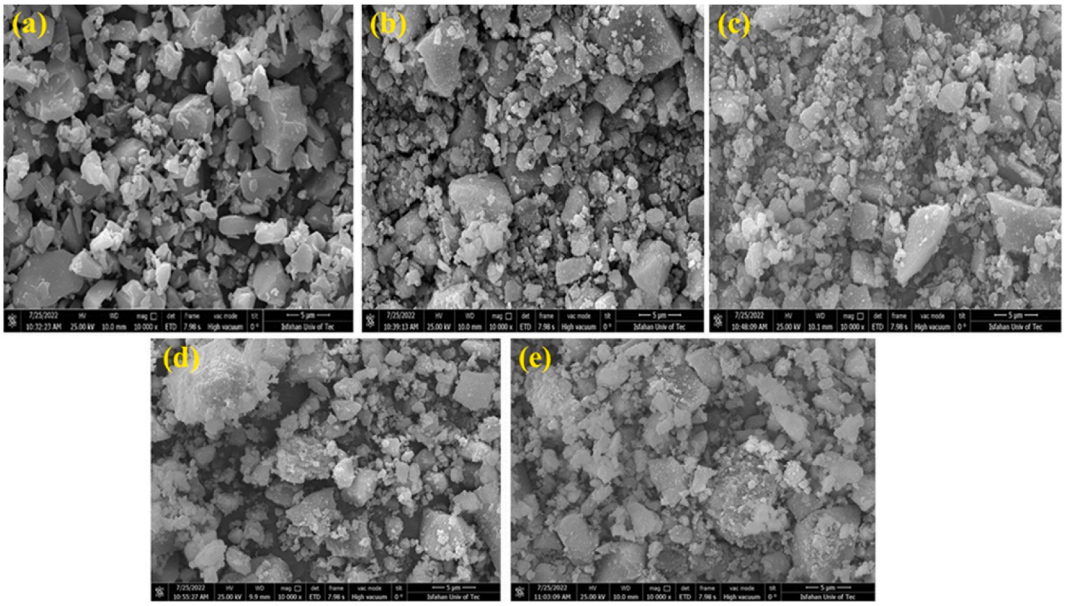

Fig. 7. FESEM with ×10000 magnification of the fabricated specimen: a) GC, b) HGC, c) HGC-ZnO 2 wt%, d) HGC-ZnO 4 wt% and e) HGC-ZnO 6 wt %, SEM analysis was conducted solely to present the morphology and microstructure of the samples, without any comparative analysis between the samples.

Table 2
Average diameter of particles obtained by FESEM images utilizing Image-J software.

Specimen name	Average particle diameter	Unit
GC	0.23	micrometer
HGC	36.06	nanometer
HGC-ZnO 2 wt%	45.081	nanometer
HGC-ZnO 4 wt%	58.01	nanometer
HGC-ZnO 6 wt%	33.900	nanometer

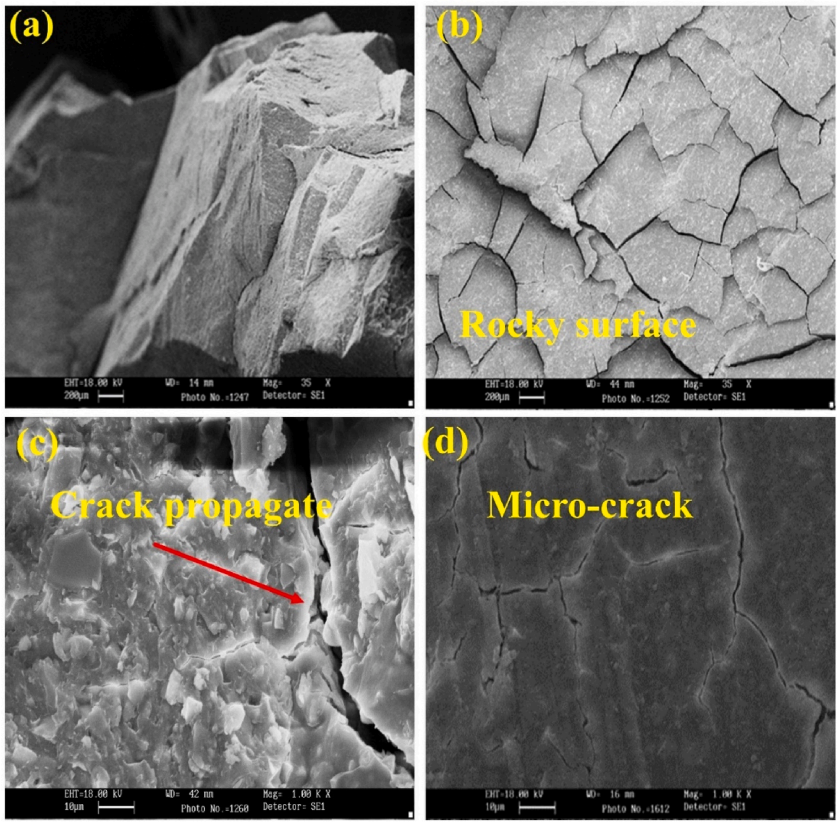

Fig. 8. SEM images of the fracture surface of the specimens; a) GC, b) HGC, c) HGC-ZnO 2 wt%, and d) HGC-ZnO 4 wt%.

Table 3
The porosity percentages of the scaffolds.

Specimen name	Porosity (%) ± 5
GC	10 %
HGC	40 %
HGC-ZnO 2 wt%	21 %
HGC-ZnO 4 wt%	30 %
HGC-ZnO 6 wt%	30 %

3.5. Mechanical strength evaluation

Certain fibers and nanoparticles can significantly enhance cement strength [22]. Nanostructures generally improve the mechanical strength and antibacterial properties of GICs, particularly in load-bearing posterior teeth [26]. Nanoparticles such as TiO_2, HA, SiO_2, ZrO_2, and Al_2O_3 enhance GIC properties by promoting a more uniform particle distribution and increasing surface area and energy [25–27]. Compressive strength tests were performed three times per specimen group for validation.

According to Fig. 9, the GC sample exhibited the highest maximum stress compared to other samples. However, the addition of HA to GC in the HGC sample resulted in lower maximum stress and compressive resistance due to HA's high porosity and low mechanical strength. Conversely, incorporating ZnO into HA increased maximum stress compared to the HGC sample. Notably, varying the ZnO content did not consistently increase maximum stress, as observed between HGC-ZnO 4 wt% and HGC-ZnO 6 wt%.

The HGC-ZnO 4 wt% sample showed the highest resistance to crushing, surpassing the control sample by 10.77 MPa. Adding HA alone weakened GC's mechanical properties, but future studies aim to enhance GC cement's mechanical properties by incorporating ZnO into HA and GC matrices (see Fig. 10).

3.6. Bioactivity evaluation

Fig. 11 illustrates bioactivity test results, showing higher calcium absorption in GC specimens up to the seventh day, followed by a gentler slope, with increased calcium absorption and fluoride ion release over time. HGC specimens exhibit relatively higher calcium

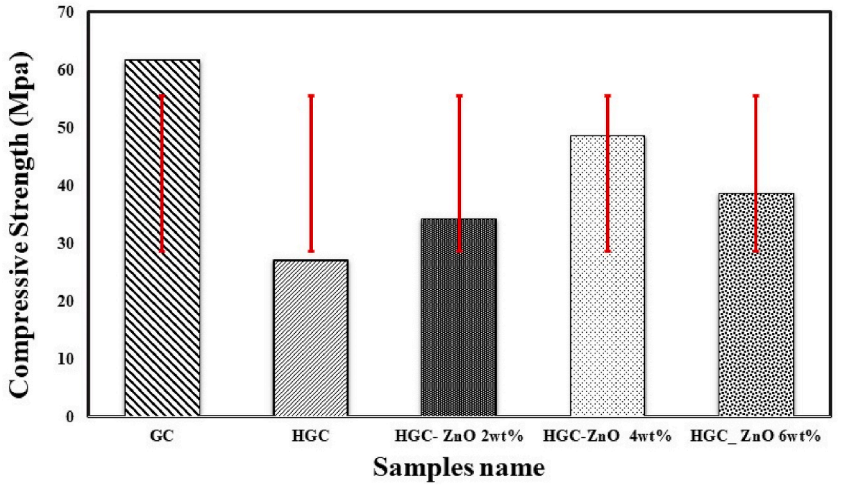

Fig. 9. Maximum stress diagram and display of SD bars of specimens GC, HGC, HGC-ZnO 2 wt%, HGC-ZnO 4 wt%, and HGC-ZnO 6 wt%.

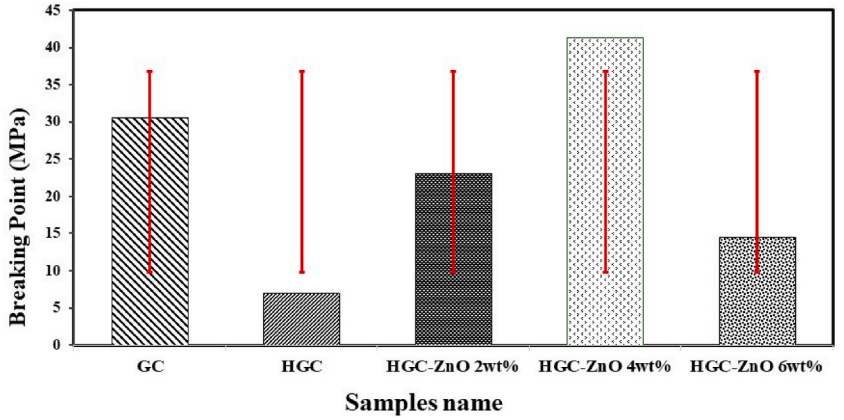

Fig. 10. Break point diagram display of SD bars of specimens GC, HGC, HGC-ZnO 2 wt%, HGC-ZnO 4 wt%, and HGC-ZnO 6 wt%.

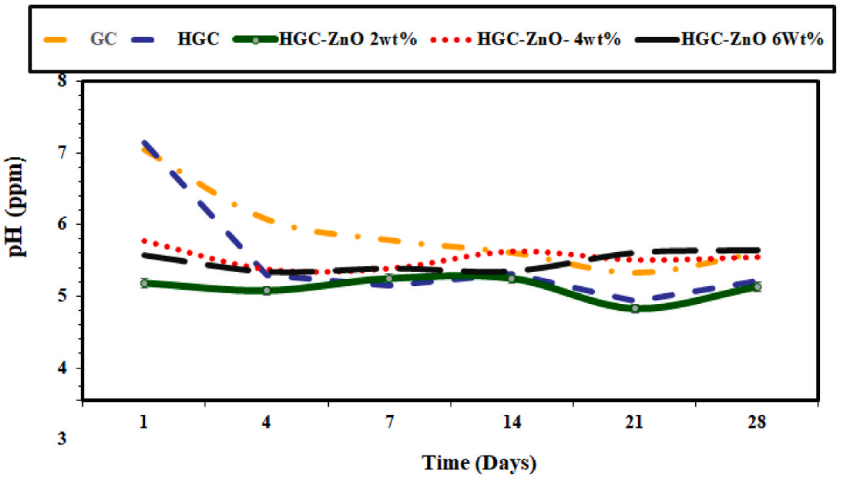

Fig. 11. Bioactivity diagram of specimens GC, HGC, HGC-ZnO 2 wt%, HGC-ZnO 4 wt% and HGC-ZnO 6 wt%.

absorption compared to GC. Increased pH correlates with fluoride ion release and calcium ion absorption. HGC-ZnO 2 wt% specimens show a slower absorption slope than HGC, followed by a phase of calcium absorption and fluoride release. HGC-ZnO 4 wt% specimens exhibit gradual calcium absorption until the fourth day, with continued absorption until the end of the period. In HGC-ZnO 6 wt% specimens, calcium absorption initially decreases compared to HGC-ZnO 4 wt%, followed by limited absorption on the 14th day and subsequent increase in calcium ion absorption and fluoride ion release in SBF solution.

Fig. 12(a–c) shows the SEM images show the surface morphology of glass-ceramic specimens after 28-day SBF immersion. Unmodified GC had minimal apatite, while heat-treated HGC and ZnO-containing HGC-ZnO samples exhibited enhanced bioactive mineral deposition, indicating the synergistic effect of heat treatment and ZnO incorporation.

Fig. 13 shows the biodegradability results according to the data from the degradation test presented in Fig. 13, the weight change index during the test process was negligible for the GC specimen. The highest average weight gain, 0.16 g, was observed for the 4 wt% HGC-ZnO specimen, indicating the apatite formation. The 2 wt% HGC-ZnO specimen showed the lowest average weight change (initial increase after 21 days, followed by a decrease by day 28th), suggesting its degradability.

Therefore, GC cement without additives exhibits minimal degradability, likely due to its low porosity. The weight gain results and apatite formation can be further validated by SEM results.

3.7. FTIR analysis

FTIR analysis was employed to identify chemical bonds, molecular interactions, and functional groups present in the materials. The analysis was conducted on specimens immersed in SBF for 28 days, with results shown in Fig. 14(a–e). In Fig. 14 (a), corresponding to the GC specimen, the vibrational bands at 3440 cm^{-1} and 1630 cm^{-1} are attributed to stretching and bending OH groups, respectively. The band at 1460 cm^{-1} corresponds to P=O groups, while the band at 1055 cm^{-1} is associated with Si-O-Si groups. Additionally, bands at 607 cm^{-1} and 451 cm^{-1} are attributed to bending Si-O and out-of-plane SiO groups, respectively. In Fig. 14 (b), representing the HGC specimen, similar vibrational bands are observed: 3440 cm^{-1} (stretching OH), 1630 cm^{-1} (bending OH), 1460 cm^{-1} (P=O), 1055 cm^{-1} (Si-O-Si), 607 cm^{-1} (bending Si-O), and 451 cm^{-1} (out-of-plane SiO). Fig. 14 (c), corresponding to the HGC-ZnO 2 wt% specimen, shows a vibrational band at 3440 cm^{-1} attributed to OH groups, and a band at 1507 cm^{-1} attributed to symmetric and asymmetric bending vibrations of C=O groups. A strong band below 700 cm^{-1} indicates Fe-O stretching modes, with specific attribution to α-Fe_2O_3.

Fig. 14 (d), corresponding to the 4 wt% HGC-ZnO specimen, displays bands at 3440 cm^{-1} (OH groups), 3000 cm^{-1} (aromatic CH), 2800 cm^{-1} (aliphatic CH stretching vibrations), 1811 cm^{-1} (carbonyl group), 1507 cm^{-1} (C=O bending), 1300 cm^{-1} (alcohol type bending), 872 cm^{-1} (CH stretching), and 510 cm^{-1} (Ti-O or Al-O groups). Fig. 14 (e), attributed to the HGC-ZnO 6 wt% specimen, shows bands in the asymmetric C=O group region, 1434 cm^{-1} (P=O group), 1300 cm^{-1} (alcohol type bending), 876 cm^{-1} (CH stretching), and 514 cm^{-1} (Ti-O or Al-O groups). These results show the diverse molecular compositions and interactions observed across the tested specimens under FTIR analysis.

3.8. Examining the amount of fluoride released in the specimens

The fluoride ions released from GC enhance mineral endurance and stability, increase antibacterial properties, and improve the absorption of GC. This ion is released over a prolonged period [11]. In this study, fluoride release was measured for up to 28 days, with results detailed in Table 4. According to Table 4, the fluoride ion release in the GC specimen increased due to the absence of other ions. The HGC-ZnO specimen showed the least reduction in fluoride release at 2 wt%, and the greatest reduction at 6 wt%, reflecting the variance in fluoride ion release due to chemical reactions. Although fluoride ions were not detected in the HGC-ZnO 6 wt% specimen in the XRF analysis, fluoride release was observed, indicating the release of fluoride ions.

By addition of HA and ZnO to the glass ionomer cement, the initial fluoride release on the first day increased from 0.72 mg/L to 0.88 mg/L compared to the control sample. However, by the 30th day, the control sample exhibited higher fluoride release than the samples containing HA and ZnO. The control sample showed a 170.97 % increase in fluoride release on the 30th day compared to the first day, while the HGC sample exhibited a negative release rate. In ZnO-containing samples, the fluoride release rate decreased compared to the first day. Furthermore, it cannot be concluded that adding ZnO and increasing its concentration reduces the fluoride release rate, as this requires a longer observation period. Despite this, due to the significant antibacterial properties of ZnO, the reduction in fluoride release is not highly critical.

3.9. Examining the antibacterial properties

3.9.1. The results of the antibiogram test by determining the aura of non-growth

The antibiogram test measures the effectiveness of antibiotics or other antimicrobial agents in inhibiting bacterial growth in a laboratory setting. The Bauer-Kirby method, which involves determining the diameter of the growth inhibition zone via disk diffusion or well diffusion, is used to assess the antimicrobial effect of substances. The specimens in this test were evaluated after 24 h, with results shown in Fig. 15(a–j).

As observed in Fig. 15(a–j), the specimens GC, HGC, HGC-ZnO 2 wt%, HGC-ZnO 4 wt%, and HGC-ZnO 6 wt% exhibited zero millimeters of growth inhibition zones against Staphylococcus and *Escherichia coli* bacteria, indicating that these bacteria are resistant to the tested substances.

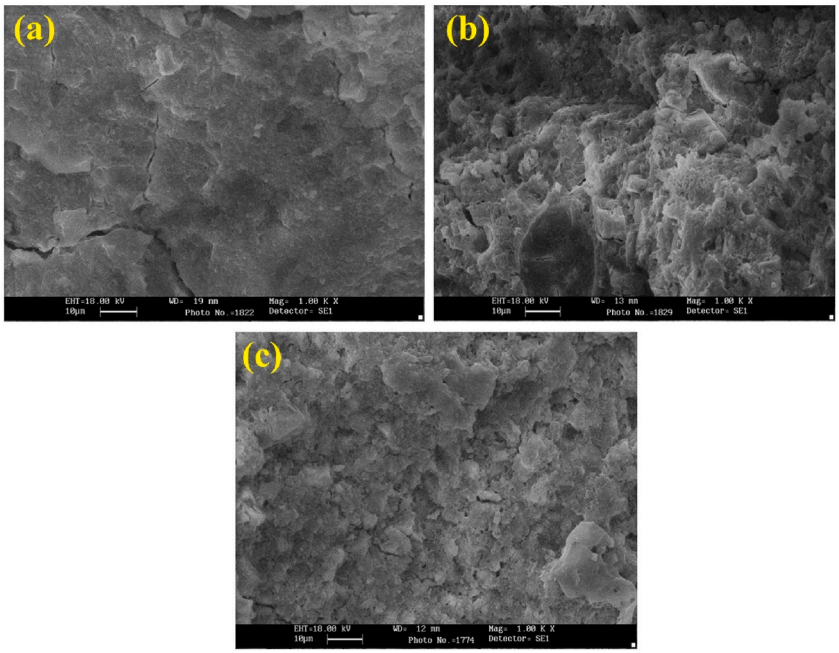

Fig. 12. SEM images of a-c) specimens after 28 days of immersion in SBF solution of samples containing various amount of ZnO nanoparticles.

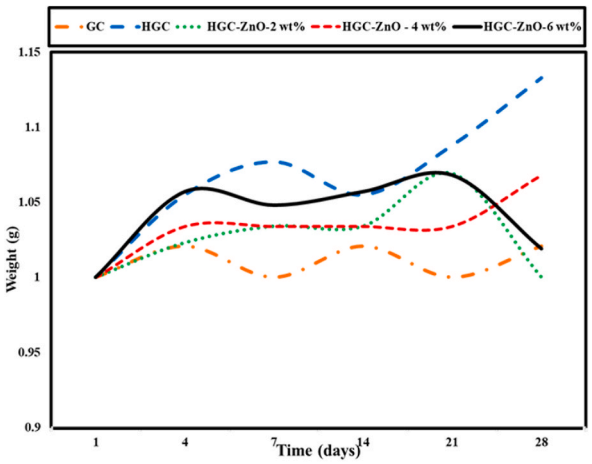

Fig. 13. Biodegradability chart of specimens GC, HGC, HGC-ZnO 2 wt%, HGC-ZnO 4 wt% and HGC-ZnO 6 wt%.

3.9.2. The results of the antibacterial layer test by MIC/MBC method

While GC cement offers bioactivity, biodegradability, and biocompatibility, it has weak antibacterial properties and insufficient load-bearing capacity. Additionally, the slow setting time of GC cement poses challenges in clinical applications. The rate of bacterial inhibition and lethality has been shown for Gram-negative and Gram-positive bacteria. They are shown in Tables 5 and 6 Fig. 16(a–j) and Fig. 17(a–j).

According to Tables 5 and 6, the tested sample has the following effects:

- For the powder samples GC, HGC, HGC-ZnO 2 wt%, HGC-ZnO 4 wt%, and HGC-ZnO 6 wt% the property of tensile strength on Staphylococcus bacteria in this 10–0.078 mg/ml does not have.
- For the powder samples GC, HGC, HGC-ZnO 2 wt%, HGC-ZnO 4 wt% and HGC-ZnO 6 wt% it has the property of inhibition and lethality on *Escherichia coli* bacteria at a concentration of 0.078–10 mg/ml.

The well diffusion test serves as a preliminary evaluation of antibacterial activity, but it is insufficient on its own to draw definitive conclusions. The test involves placing the sample in a solid agar medium, where the antibacterial effect depends on the substance's

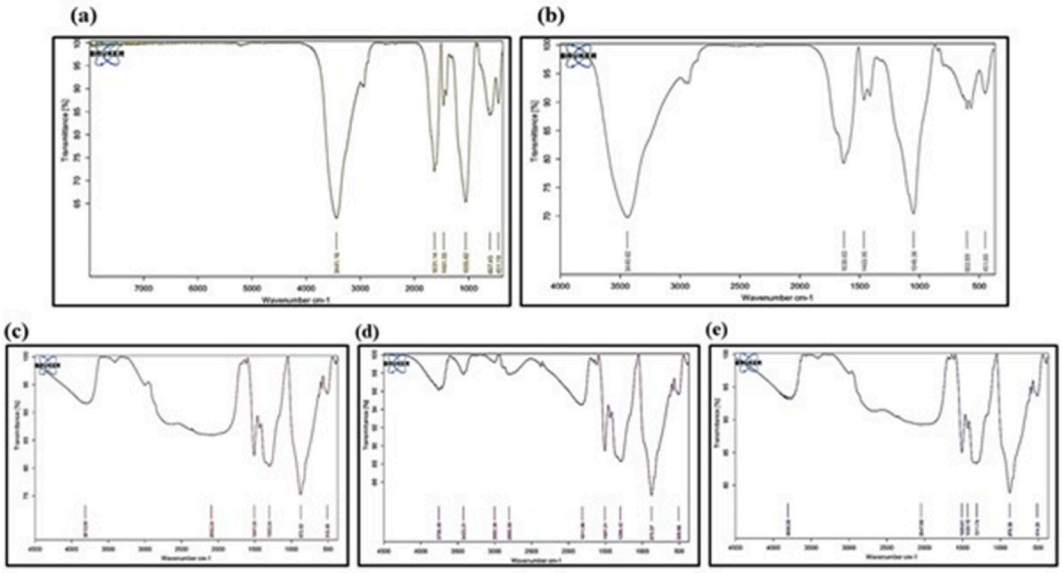

Fig. 14. FTIR analysis after 28 days of immersion in SBF solution; a) GC, b) HGC, c) HGC-ZnO 2 wt%, d) HGC-ZnO 4 wt% and e) HGC-ZnO 6 wt%.

Table 4
Fluoride release rate.

Specimen name	Fluoride released on 1st day (mg/l)	Fluoride released on 30th day (mg/l)	Fluoride change rate (%)
GC	0.31	0.84	97.170
HGC	1.13	0.8	−29.2
HGC-ZnO 2 wt%	1.03	1.02	0.97
HGC-ZnO 4 wt%	1.19	0.9	−24.37
HGC-ZnO 6 wt%	1.15	0.73	36.52

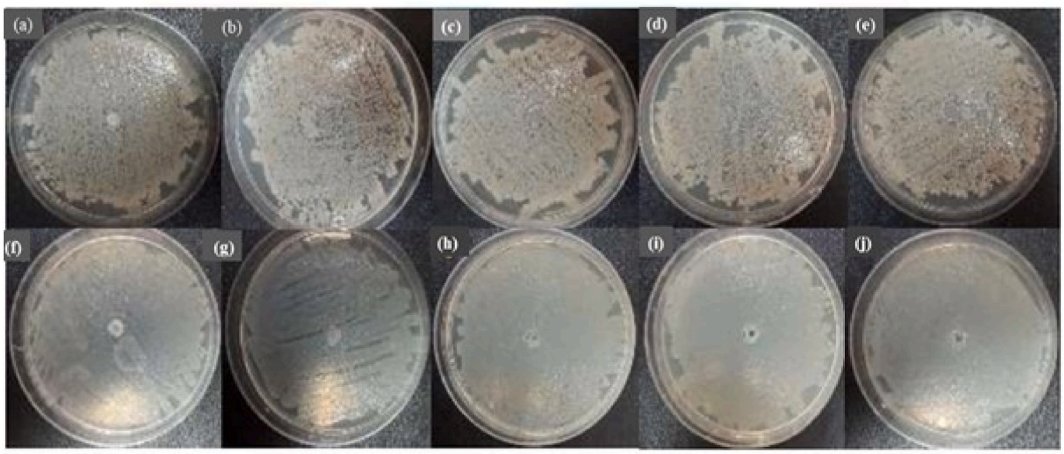

Fig. 15. Antibiogram test by determining the non-growth halo for GC, HGC, HGC-ZnO 2 wt%, HGC-ZnO 4 wt%, HGC-ZnO 6 wt% specimens in each test plate for Staphylococcus and *Escherichia coli* a–e: a) GC, b) HGC, c) HGC-ZnO 2 wt%, d) HGC-ZnO 4 wt%, HGC-ZnO 6 wt% (e by well diffusion method on Staphylococcus, f–j: specimen f) GC, g) HGC, h) HGC-ZnO 2 wt %, i) HGC-ZnO 4 wt%, HGC-ZnO 6 wt% (j) by well diffusion method on *Escherichia coli*.

ability to diffuse through the medium. In contrast, the Minimum Inhibitory Concentration (MIC) and Minimum Bactericidal Concentration (MBC) tests are performed in liquid media and provide a more accurate measure of the concentration needed to inhibit or kill bacteria. A substance that performs well in a solid environment, as indicated by the well diffusion test, may not necessarily be as

Table 5
MIC and MBC tests results (*Staphylococcus aureus* bacteria), for the concentration of 0.078–10 mg/ml from samples GC, HGC, HGC-ZnO 2 wt%, HGC-ZnO 4 wt% and HGC-ZnO 6 wt%.

From samples GC, HGC, HGC-ZnO 2 wt%, HGC-ZnO 4 wt% and HGC-ZnO 6 wt%.									Control positive	Control negative
Pipe number	10	5	2.5	1.25	0.625	0.312	0.156	0.078		
MIC	+	+	+	+	+	+	+	+	+	–
MBC	+	+	+	+	+	+	+	+	+	–

Table 6
MIC and MBC test results of samples in each test tube (*Escherichia coli* bacteria) for concentration 10–0.078 mg/ml from the samples GC, HGC, HGC-ZnO 2 wt%, HGC-ZnO 4 wt% and HGC-ZnO 6 wt%.

From samples GC, HGC, HGC-ZnO 2 wt%, HGC-ZnO 4 wt% and HGC-ZnO 6 wt%.									Control positive	Control negative
Pipe number	10	5	2.5	1.25	0.625	0.312	0.156	0.078		
Test MIC	+	+	+	+	+	+	+	+	+	–
Test MBC	+	+	+	+	+	+	+	+	+	–

Fig. 16. Antibacterial test (MIC): (a–e) depict the effect of the powder sample at eight different concentrations on *Staphylococcus* bacteria, with positive and negative controls displayed on the left of each image. The samples are numbered 1 to 8, corresponding to concentrations of 10, 5, 2.5, 1.25, 0.625, 0.312, 0.156, and 0.078 mg/ml, respectively. (f–j) show the effect of the powder sample on *Escherichia coli* bacteria under the same eight concentrations, with positive and negative controls also shown on the left of each image.

effective in a liquid environment, as shown by the MIC and MBC tests. These tests are crucial for determining the precise antibacterial concentrations in a liquid medium, which may reveal that a substance with inhibitory effects in solid media is not as effective in liquid conditions. Although these experiments primarily focus on evaluating the antibacterial performance of the modified glass cement, it acknowledges the critical role of Zn^{2+} ion release in determining long-term antibacterial efficacy. Future studies should include a comprehensive analysis of Zn^{2+} ion release over extended periods, particularly in SBFs, to fully understand its impact on the material's performance.

3.10. Analysis of the cytotoxicity results for the specimens

Bone cement and biocompatible scaffolds can cause chronic inflammation, leading to tissue rejection or necrosis. Therefore, in tissue engineering, it is preferable to use biodegradable scaffolds that are non-toxic and produce non-toxic degradation products [33, 34]. The cytotoxicity MTT assay measures the biocompatibility of the specimens. Figs. 18 and 19(a–o), indicate that the percentage of

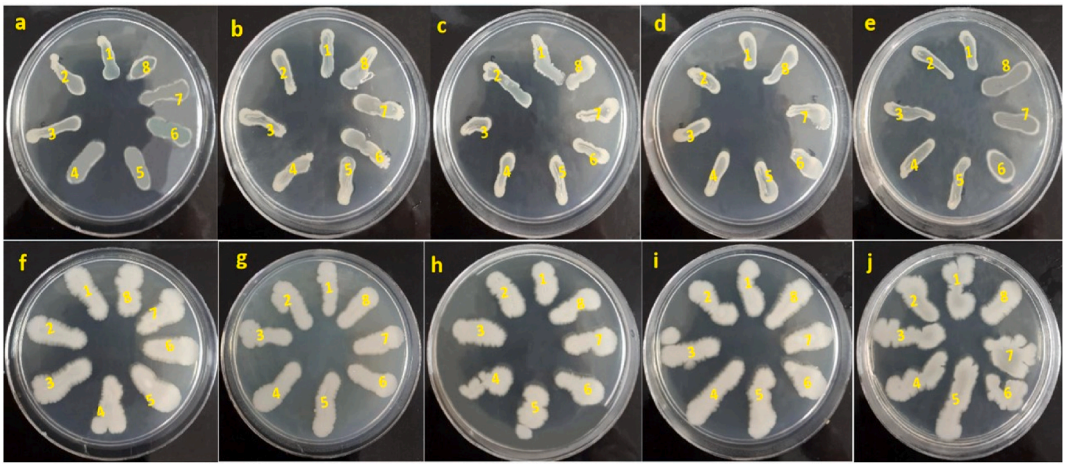

Fig. 17. Antibacterial test (MBC): (a–e) show *Staphylococcus* bacteria exposed to the powder sample at eight different concentrations, with samples numbered 1 to 8 corresponding to concentrations of 10, 5, 2.5, 1.25, 0.625, 0.312, 0.156, and 0.078 mg/ml (f–j) depict **Escherichia coli* bacteria exposed to the same powder sample at the same eight concentrations, with samples similarly numbered from 1 to 8, representing concentrations of 10, 5, 2.5, 1.25, 0.625, 0.312, 0.156, and 0.078 mg/ml.

cell viability in contact with the test specimen was compared to the control specimen. The HGC-ZnO 2 wt%, HGC-ZnO 4 wt%, and HGC-ZnO 6 wt% specimens showed no toxicity to MG 63 cells after 24 ± 2, 48 ± 2, and 72 ± 2 h.

The HA addition to the GC structure reduces mechanical properties and cytotoxicity lasting up to 24 h. However, the ZnO addition increases mechanical strength, calcium production and growth, and eliminates cytotoxicity. Based on the summarized results, the HGC-ZnO 4 wt% specimen is recommended as the preferred choice for the treatment and improvement of bone diseases.

4. Conclusion

In this study, we successfully enhanced the mechanical and biological properties of GIC by reinforcing it with HA and ZnO nanoparticles. The incorporation of HA and ZnO significantly improved the bioactivity, mechanical strength, and antibacterial properties of the GC. Specifically, the addition of 4 wt% ZnO resulted in the highest increase in compressive strength, while maintaining a favorable cytocompatibility profile. However, the fluoride release was reduced in the HA-ZnO reinforced samples, which suggests a trade-off between mechanical enhancement and fluoride ion release. The results of this study suggest that HA and ZnO reinforcement can create a more robust and biologically active cement suitable for dental and orthopedic applications, providing a promising approach for improving the performance of bone and dental cements. Future studies should further investigate the long-term effects of Zn^{2+} ion release and its impact on the antibacterial efficacy over extended periods to fully establish the clinical relevance of these materials. The HGC-ZnO 4 wt% specimen exhibited the best performance, achieving compressive strength (10.77 MPa

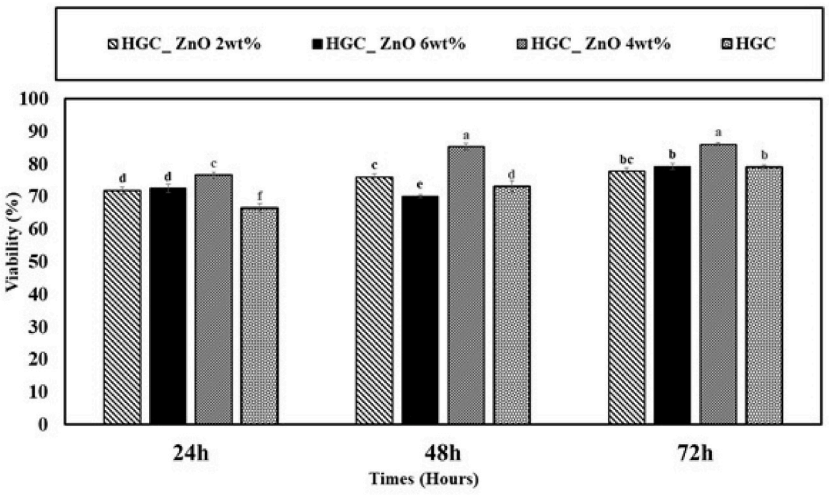

Fig. 18. Cytotoxicity chart of HGC specimens, HGC-ZnO 2 wt%, HGC-ZnO 4 wt% and HGC-ZnO 6 wt%.

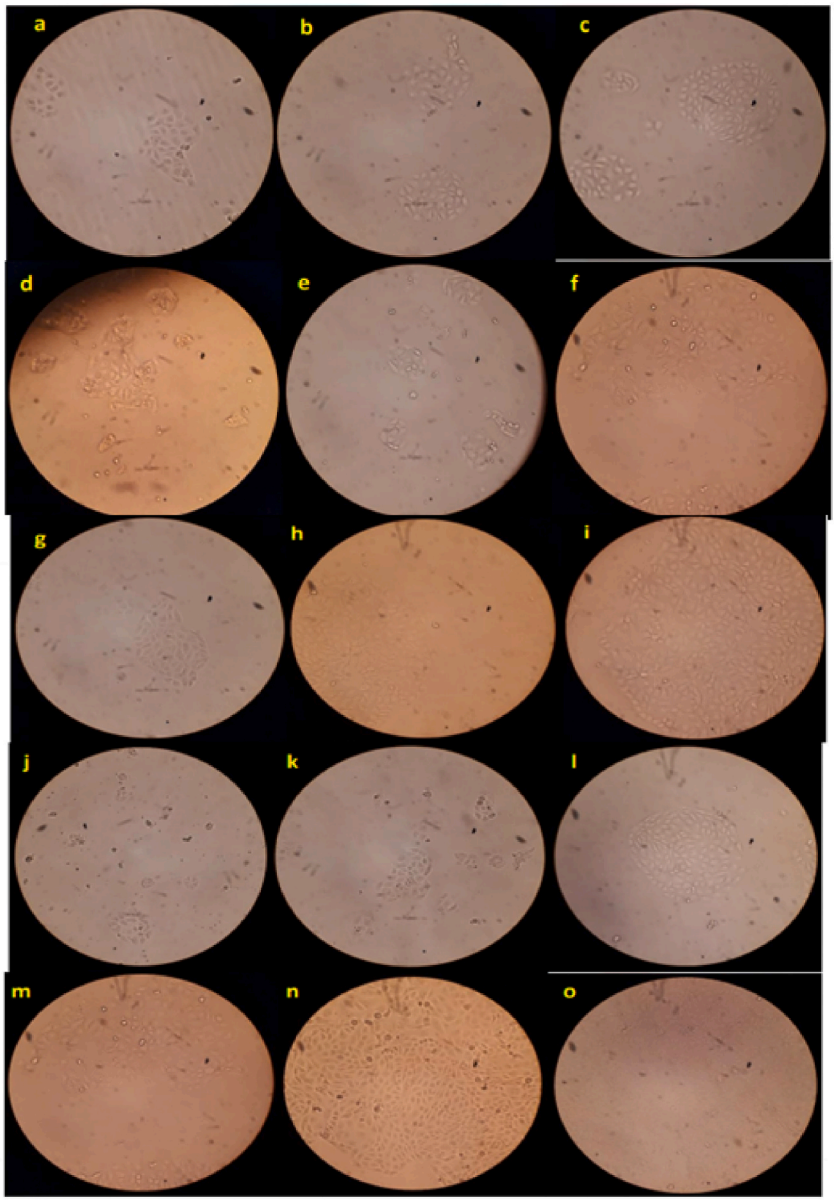

Fig. 19. Image of cells after exposure to specimens of HGC, HGC-ZnO 2 wt%, HGC-ZnO 4 wt%, HGC-ZnO 6 wt%, and control after a period of 24 ± 2, 48 ± 2 and 72 ± 2 h **a-c)** specimen HGC-ZnO 2 wt% after a period of 24 ± 2, 48 ± 2 and 72 ± 2 h, f-d) HGC-ZnO 6 wt% specimen after a period of 24 ± 2, 48 ± 2 and 72 ± 2 h, **i-g)** specimen HGC-ZnO 4 wt% after a period of 24 ± 2, 48 ± 2 and 72 ± 2 h**, l-j)** HGC specimen after a period of 24 ± 2, 48 ± 2 and 72 ± 2 h, **o-m)** control specimen after a period time, 24 ± 2, 48 ± 2 and 72 ± 2 h.

increase over control), 40 % higher calcium absorption, and over 90 % cell viability, despite a 24.37 % reduction in fluoride release. These significant improvements in mechanical, bioactive, and antibacterial properties make this modified cement the preferred choice for dental and orthopedic applications.

CRediT authorship contribution statement

Reyhaneh Azimi: Writing – original draft, Data curation, Conceptualization. **Mohamad Shahgholi:** Visualization, Supervision. **Amirsalar Khandan:** Writing – review & editing, Validation.

Availability of data and materials

The datasets supporting the conclusions of this study are included within the article.

Declaration of competing interest

The authors declare that they have no known competing financial interests or personal relationships that could have appeared to influence the work reported in this paper.

References

[1] M.P. Ferraz, An overview on the big players in bone tissue engineering: biomaterials, scaffolds and cells, Int. J. Mol. Sci. 25 (7) (2024 Mar 29) 383.
[2] J.J. Lee, Y.K. Lee, B.J. Choi, J.H. Lee, H.J. Choi, H.K. Son, S.O. Kim, Physical properties of resin-reinforced glass ionomer cement modified with micro and nano-hydroxyapatite, J. Nanosci. Nanotechnol. 10 (8) (2010) 5270–5276.
[3] A. Gupta, D. Singh, P. Raj, H. Gupta, S. Verma, S. Bhattacharya, Investigation of ZnO-hydroxyapatite nanocomposite incorporated in restorative glass ionomer cement to enhance its mechanical and antimicrobial properties, J. Bionanoscience 9 (3) (2015) 190–196.
[4] R. Cruz, J. Calasans-Maia, S. Sartoretto, V. Moraschini, A.M. Rossi, R.S. Louro, M.D. Calasans-Maia, Does the incorporation of zinc into calcium phosphate improve bone repair? A systematic review, Ceram. Int. 44 (2) (2018) 1240–1249.
[5] S. Pina, J.M. Ferreira, Brushite-forming Mg-, Zn-and Sr-substituted bone cements for clinical applications, Materials 3 (1) (2010) 519–535.
[6] P. Balasubramanian, L.A. Strobel, U. Kneser, A.R. Boccaccini, Zinc-containing bioactive glasses for bone regeneration, dental and orthopedic applications, Biomedical glasses 1 (1) (2015).
[7] Z. He, Q. Zhai, M. Hu, C. Cao, J. Wang, H. Yang, B. Li, Bone cements for percutaneous vertebroplasty and balloon kyphoplasty: current status and future developments, Journal of orthopaedic translation 3 (1) (2015) 1–11.
[8] I.H. Suparto, E. Kurniawan, Synthesis and characterization of hydroxyapatite-zinc oxide (HAp-ZnO) as antibacterial biomaterial, in: IOP Conference Series: Materials Science and Engineering, vol. 599, IOP Publishing, 2019, August 012011, 1.
[9] R. Fada, M. Shahgholi, R. Azimi, et al., Estimation of porosity effect on mechanical properties in calcium phosphate cement reinforced by strontium nitrate nanoparticles: fabrication and FEM analysis, Arabian J. Sci. Eng. 49 (2024) 1815–1825.
[10] L. Ciołek, M. Chraniuk, P. Bollin, M. Biernat, M. Panasiuk, D. Nidzworski, E. Pamuła, Bioactive glasses enriched with zinc and strontium: synthesis, characterization, cytocompatibility with osteoblasts and antibacterial properties, Acta Bioeng. Biomech. 25 (4) (2024) 69–80.
[11] Shakour Shojaei, Mohamad Shahgholi, Arash Karimipour, The effects of atomic percentage and size of Zinc nanoparticles, and atomic porosity on thermal and mechanical properties of reinforced calcium phosphate cement by molecular dynamics simulation, J. Mech. Behav. Biomed. Mater. 141 (2023) 105785.
[12] S. Rahnama, F. Bahraini, S.P. Mirmalek, R. Jalalian, E. Fardi, S. Jamali, Evaluation of the effects of cinnamon, CuO, and ZnO nanoparticles on the antibacterial properties of a luting glass ionomer orthodontic bands cements. A Systematic Review and Meta-Analysis, ACADEMIC JOURNAL, 2024.
[13] R.A. Alatawi, N.H. Elsayed, W.S. Mohamed, Influence of hydroxyapatite nanoparticles on the properties of glass ionomer cement, J. Mater. Res. Technol. 8 (1) (2019) 344–349.
[14] F. Angelieri, Y.S. da Silva, D.A. Ribeiro, Genotoxicity and cytotoxicity induced by eluates from orthodontic glass ionomer cements in vitro, The Saudi dental journal 30 (1) (2018) 38–42.
[15] S.C. Isler, G. Ozcan, M. Ozcan, H. Omurlu, Clinical evaluation of combined surgical/restorative treatment of gingival recession-type defects using different restorative materials: a randomized clinical trial, Journal of dental sciences 13 (1) (2018) 20–29.
[16] G.J. Mount, W.R. Hume, Preservation and Reconstruction of Tooth Structure, Mosby International Ltd, 1998.
[17] I.R. Bordea, S. Candrea, G.T. Alexescu, S. Bran, M. Băciuț, G. Băciuț, D.A. Todea, Nano-hydroxyapatite use in dentistry: a systematic review, Drug Metab. Rev. 52 (2) (2020) 319–332.
[18] H.S. Ching, N. Luddin, T.P. Kannan, I. Ab Rahman, N.R. Abdul Ghani, Modification of glass ionomer cements on their physical-mechanical and antimicrobial properties, J. Esthetic Restor. Dent. 30 (6) (2018) 557–571.
[19] Z. Beyene, R. Ghosh, Effect of zinc oxide addition on antimicrobial and antibiofilm activity of hydroxyapatite: a potential nanocomposite for biomedical applications, Mater. Today Commun. 21 (2019) 100612.
[20] P.V. Gnaneshwar, S.V. Sudakaran, S. Abisegapriyan, J. Sherine, S. Ramakrishna, M.H.A. Rahim, J.R. Venugopal, Ramification of zinc oxide doped hydroxyapatite biocomposites for the mineralization of osteoblasts, Mater. Sci. Eng. C 96 (2019) 337–346.
[21] N. Ohtsu, Y. Kakuchi, T. Ohtsuki, Antibacterial effect of zinc oxide/hydroxyapatite coatings prepared by chemical solution deposition, Appl. Surf. Sci. 445 (2018) 596–600.
[22] J.W. Nicholson, S.K. Sidhu, B. Czarnecka, Enhancing the mechanical properties of glass-ionomer dental cements: a review, Materials 13 (11) (2020) 2510.
[23] M. Bilić-Prcić, V.B. Rajić, A. Ivanišević, A. Pilipović, S. Gurgan, I. Miletić, Mechanical properties of glass ionomer cements after incorporation of Marine Derived Hydroxyapatite, Materials 13 (16) (2020) 3542.
[24] S. Padmaja, J. Somasundaram, V. Sivaswamy, Nano glass ionomers-A review, Indian Journal of Forensic Medicine & Toxicology 14 (4) (2020).
[25] I.A. Moheet, N. Luddin, I. Ab Rahman, T.P. Kannan, N.R.N. Abd Ghani, S.M. Masudi, Modifications of glass ionomer cement powder by addition of recently fabricated nano-fillers and their effect on the properties: a review, Eur. J. Dermatol. 13 (3) (2019) 470–477.
[26] F. Amin, S. Rahman, Z. Khurshid, M.S. Zafar, F. Sefat, N. Kumar, Effect of nanostructures on the properties of glass ionomer dental restoratives/cements: a comprehensive narrative review, Materials 14 (21) (2021) 6260.
[27] E. Gjorgievska, J.W. Nicholson, D. Gabrić, Z.A. Guclu, I. Miletić, N.J. Coleman, Assessment of the impact of the addition of nanoparticles on the properties of glass–ionomer cements, Materials 13 (2) (2020) 276.
[28] C.F. Burmeister, A. Kwade, Process engineering with planetary ball mills, Chem. Soc. Rev. 42 (18) (2013) 7660–7667.
[29] V.S. Rakshitha, J.L. Prabha, D.P. Antony, Assessment of occlusal load strength of glass ionomer cement and composite in class V cavities: an in-vitro study, Cureus 15 (11) (2023).
[30] S. Saha, S. Pal, Mechanical properties of bone cement: a review, J. Biomed. Mater. Res. 18 (4) (1984) 435–462.
[31] C.J. Koh, A. Atala, Tissue engineering, stem cells, and cloning: opportunities for regenerative medicine, J. Am. Soc. Nephrol. 15 (5) (2004) 1113–1125.
[32] L.E. Freed, G. Vunjak-Novakovic, Tissue engineering bioreactors, Principles of tissue engineering 2 (2000) 143–156.
[33] Y. Cao, et al., Scaffolds, stem cells, and tissue engineering: a potent combination, Aust. J. Chem. 58 (10) (2005) 691–703.
[34] A. Attaeyan, M. Shahgholi, A. Khandan, Fabrication and characterization of novel 3D porous Titanium-6Al-4V scaffold for orthopedic application using selective laser melting technique, Iran. J. Chem. Chem. Eng.(IJCCE) Research Article 43 (1) (2024).